Possible thermodynamic stability and superconductivity of antifluorite $Be_2B_xC_{1-x}$

Jonathan E. Moussa,* Jesse Noffsinger, and Marvin L. Cohen
Department of Physics, University of California at Berkeley, Berkeley, California 94720, USA
and Materials Sciences Division, Lawrence Berkeley National Laboratory, Berkeley, California 94720, USA
(Received 30 April 2008; revised manuscript received 9 July 2008; published 10 September 2008)

The $Be_2B_xC_{1-x}$ alloy in the antifluorite structure is theoretically studied as a possible superconductor. Although both Be_2B and Be_2C terminal phases are experimentally observed to be thermodynamically stable, our calculations suggest that the stability of the Be_2B phase requires a high concentration of defects. The carbon-rich limit is expected to contain few defects and we predict the alloy to be thermodynamically accessible in the range $0 \leq x \leq 0.25$. The superconducting T_c is predicted to increase with boron concentration with a value of 3–8 K at $x=0.25$ and a plateau of 5–13 K for $x>0.4$. The uncertainty in this prediction results from a small electron-phonon coupling of $\lambda \leq 0.5$ over the entire range of boron concentration. The material remains in the weak-coupling regime of superconductivity where T_c is sensitive to small variations in λ and μ^*.

DOI: 10.1103/PhysRevB.78.104506 PACS number(s): 74.10.+v, 74.62.Dh, 74.70.Dd

I. INTRODUCTION

Following the discovery of superconductivity in MgB_2 at 40 K (Ref. 1) and boron-doped diamond at 4 K,[2] the theoretical and experimental search for new superconductors has partly focused on structurally and chemically related materials. Superconductivity has since been experimentally realized in analogs of boron-doped diamond, in both boron-doped silicon[3] and silicon carbide.[4] With the incorporation of boron into diamond beyond its solubility limit, the T_c has experimentally[5] reached 11 K at 5% boron concentration and is predicted[6] to surpass 55 K at even higher boron concentrations. Boron doping has also been suggested as a possible mechanism for superconductivity predicted[7] in boron carbide, which can be synthesized over a wide range of boron-carbon stoichiometries. Superconducting structural analogs of MgB_2 such as LiB (Ref. 8) and $Li_{1-x}BC$ (Ref. 9) have also been theoretically proposed, but have not yet been experimentally realized.

While electron-phonon superconductivity is theoretically understood enough to predict transition temperatures,[10] such predictions are often limited by an inability to synthesize or characterize materials. In the case of boron-doped diamond, the prediction[6] of T_c enhancement with increased doping assumes that all boron is incorporated substitutionally. Other boron-based diamond defects have been theoretically proposed[11] and experimental NMR studies[12] have shown that not all boron dopants act as an acceptor in diamond. In the case of boron carbide, the variation in boron-carbon stoichiometry is believed[13] to be related to a high concentration of structural defects that are detrimental to a metallic state and superconductivity. In the case of LiBC, several methods have been used to remove lithium, but superconductivity has not been observed.[14] A proposed explanation[14] of this failure is the energetically-favorable reordering of boron and carbon that changes the electronic states at the Fermi level. In all three cases, an insulating crystal is theoretically expected to be driven metallic by specific desired and expected defects. However, the materials as-synthesized are complicated by other experimentally unavoidable defects.

The prediction of a new superconductor that is experimentally accessible is a difficult materials problem. The easiest approach would be to identify a known compound or small modification thereof that has been experimentally overlooked as a superconductor. Otherwise, one is left with the difficult task of determining that a new material is either thermodynamically stable or reasonably accessible by known or plausible nonequilibrium synthesis techniques. If the material is expected to have a large concentration of structural defects, these also must be taken into consideration when studying superconducting properties. In this paper, we continue to use the design paradigm of doping a parent insulator and the specific choice of boron-carbon substitutions. The specific parent insulator that we choose is Be_2C, which crystallizes in the antifluorite structure. The primary reason for this choice is that both Be_2B and Be_2C are experimentally observed to be thermodynamically stable in the antifluorite structure in the temperature range 1300–1800 K.[15] The stability of the terminal phases suggests that alloys of Be_2B and Be_2C may be thermodynamically accessible over a wide range of concentrations, in contrast to the limited solubility of boron in diamond.[2] However, one experimental report[16] finds the Be_2B phase to actually have the stoichiometry $Be_{2.8}B$, presumably from defects. The Be_2C phase can be synthesized as single-crystal film with no observed defects.[17] Alloying may serve an additional purpose of reducing the concentration of defects as the carbon concentration is increased.

Be_2B in the antifluorite structure has already been proposed as a possible superconductor.[18] The chemical flexibility of the $Be_2B_xC_{1-x}$ alloy allows the electronic properties at the Fermi surface to be further tuned so as to maximize the superconducting T_c. The antifluorite structure is formally ionic, with Be^{2+} cations and B^{4-} or C^{4-} anions, but the reduced electronegativity difference between Be and B leads to some covalent character.[19] In this configuration, carbon has a filled shell and Be_2C is an insulator,[20] while Be_2B has partially filled $2p$ bands that are metallic.[18] Boron substituted for carbon within the antifluorite structure is expected to act as an acceptor, leading to an incomplete filling of the valence bands and a metallic state.

Here we calculate and discuss both the superconducting properties and thermodynamic stability of antifluorite $Be_2B_xC_{1-x}$ for stoichiometries in the range $0 \geq x \geq 1$. In Sec.

II, the computational techniques used in this study are outlined, which are all based on the standard density-functional theory (DFT) framework. In Sec. III, electronic and structural properties of $Be_2B_xC_{1-x}$ are computed. The effects of boron-carbon disorder are observed to be small and boron doping is well described by rigid-band doping of Be_2C. In Sec. IV, the thermodynamic stability of the antifluorite $Be_2B_xC_{1-x}$ phase is assessed by considering decomposition toward known phases of the Be-B-C ternary phase diagram. We confirm that defect-free Be_2B is not thermodynamically stable in the experimentally observed temperature range, requiring the presence of unknown defects to further lower its free energy. The accessible concentration regime of the $Be_2B_xC_{1-x}$ alloy synthesized at high temperatures is estimated to be $0 \leq x \leq 0.25$. In Sec. V, the superconducting properties of $Be_2B_xC_{1-x}$ are calculated. The T_c is predicted to increase with boron concentration, attaining a value of 3–8 K at $x=0.25$ and reaching a plateau at 5–13 K for $x>0.4$.

II. COMPUTATIONAL METHODOLOGY

The most common first-principles computational approaches in condensed matter physics are DFT for the normal ground state of materials and Migdal-Eliashberg theory[21] for the superconducting state. Unless otherwise noted, all DFT calculations are performed here within the plane wave and pseudopotential formalism using the VASP computer program[22] with projector augmented wave (PAW) pseudopotentials[23] and the PBE exchange-correlation functional.[24] The superconducting gap is assumed to be isotropic. This approximation is justified based on the similarity[25] of the electronic structure of Be_2C to diamond, which is believed to have an isotropic superconducting gap.[26] Isotropy reduces the dependence of T_c to only a few parameters—$\omega_{\log}$, λ, and μ^*—according to the Allen-Dynes modification of the McMillan formula.[27] Both $\omega_{\log}$ and λ are computed from the isotropic Eliashberg spectral function $\alpha^2F(\omega)$ that is calculated from first principles. The range of μ^* values in typical free-electron-like metals[28] is 0.09–0.12, which will lead to an uncertainty in T_c that is proportional to the uncertainty from other theoretical and computational errors. A typical value of $\mu^*=0.1$ will be used for predictions made in this paper.

To account for the effects of disorder caused by the random distribution of boron and carbon in $Be_2B_xC_{1-x}$, we employ the formalism developed for studying disorder in boron-doped diamond.[6] The main approximation of this formalism beyond isotropic Eliashberg theory is that the spectral function can be approximated by using only Γ-point electron-phonon properties,

$$\alpha^2F_\Gamma(\omega) \equiv \sum_{m,n\mathbf{k}} |g^m_{n\mathbf{k},n\mathbf{k}}|^2 \delta(\epsilon_F - \epsilon_{n\mathbf{k}}) \delta(\omega - \omega^0_m). \quad (1)$$

In this equation, ω^0_m are phonon frequencies at Γ, $g^m_{n\mathbf{k},n\mathbf{k}}$ are the standard electron-phonon matrix elements evaluated for $\mathbf{k}=\mathbf{k}'$, and $\epsilon_{n\mathbf{k}}$ are electronic band energies sampled over the Brillouin zone. The $g^m_{n\mathbf{k},n\mathbf{k}}$ matrix elements can be computed directly from the deformation potentials $d\epsilon_{n\mathbf{k}}/d\mathbf{R}_i$ and require no additional integrations. If Eq. (1) is applied to a supercell of the original unit cell, then more phonon modes of the crystal are folded to the Γ point and the approximation is improved. It is crucial to test convergence with respect to unit-cell size and compare with more exact electron-phonon calculations, as this approach has been shown[29] to have poor convergence in some systems, such as aluminum. The accuracy of this approach for $Be_2B_xC_{1-x}$ is tested in Sec. V. This formalism enables inexpensive calculations of the superconducting properties of systems with large unit cells, allowing us to approximate substitutional disorder with random substitutions inside a large supercell.

A known deficiency of the $\alpha^2F_\Gamma(\omega)$ approximation is that it poorly represents coupling to acoustic phonons because the frequency and electron-phonon coupling to the acoustic modes are both zero at the Γ point. Whether or not acoustic phonons play a role in superconductivity in $Be_2B_xC_{1-x}$ is unknown. To gauge the accuracy of $\alpha^2F_\Gamma(\omega)$, the exact isotropic spectral function $\alpha^2F(\omega)$ is calculated using the Wannier function formalism[30] for high-accuracy sampling of both electrons and phonons within the Brillouin zone. Because of the substantial computational cost of this approach, it is only used for a few representative structures with small unit cells. Wannier-based calculations are performed with the PWSCF computer program[31] using norm-conserving pseudopotentials and the local-density approximation (LDA) exchange-correlation functional.

In order to compare the relative thermodynamic stability of competing structural phases and predict structural transition temperatures, free energies must be calculated as a function of temperature. The free energy of an ordered solid is composed of electronic and static lattice contributions that are calculated from ground-state DFT calculations of cohesive energy and the vibrational free energy of the lattice. For disordered materials, the free energy has an additional configurational entropy contribution. The temperature dependence of the electronic contribution to the free energy is neglected. The zero-temperature value is accurate to within a few meV per atom for the materials and temperatures considered here. Anharmonic lattice corrections are neglected, which include the temperature dependence of the phonon spectrum and lattice expansion. Anharmonic effects have been shown[32] to be required for free-energy calculations of materials that are structurally unstable at low temperatures. All materials considered in this paper are structurally stable at zero temperature.

The vibrational free-energy contribution of a phonon mode of frequency ω at temperature T is

$$F_{\text{phonon}} = \frac{1}{2}\hbar\omega + k_BT \ln(1 - e^{-\hbar\omega/k_BT}). \quad (2)$$

The total vibrational free energy per unit cell is approximated by summing over the Γ-point phonon modes, each approximating the contribution from its respective phonon branch. The zero value of the acoustic modes at the gamma point leads to an erroneous divergent contribution to the free energy that should be canceled by a vanishing phonon density of states at zero frequency. To approximate the free-energy contribution of the acoustic modes, we use the frequency of smallest, nonzero Γ-point mode. Previous studies

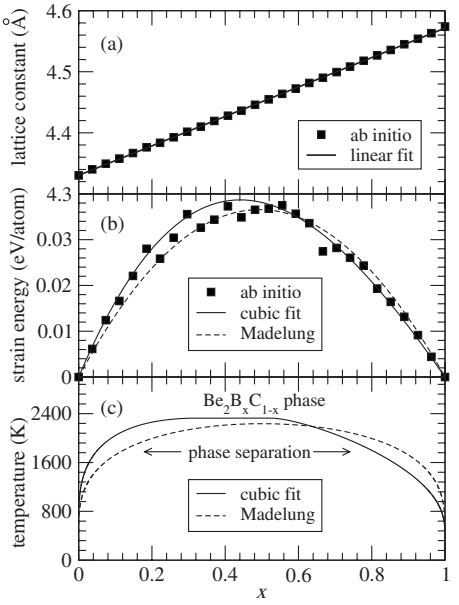

FIG. 1. Calculated structural properties of antifluorite $Be_2B_xC_{1-x}$: (a) lattice constants and a least-squares linear fit, (b) strain energy, contribution from the Madelung energy, and a least-squares cubic fit, and (c) the mixing-separation phase diagram constructed from two models of the strain energy.

of vibrational free energy[33] have demonstrated that the dominant contribution is from high-frequency modes, which justifies this crude treatment of the acoustic branches. For example, if the phonon density of states is approximated to be linear in frequency, the frequency-dependent contribution to the free energy attains its largest negative value near $0.4k_BT$ and is positive and increasing beyond k_BT.

III. STRUCTURAL AND ELECTRONIC PROPERTIES

All calculations of the antifluorite $Be_2B_xC_{1-x}$ alloy are performed on the same set of 28 test structures. Each structure is a $3\times3\times3$ supercell of the primitive antifluorite unit cell, which allows for the study of 28 stoichiometries ranging from $Be_{54}C_{27}$ to $Be_{54}B_{27}$. For each stoichiometry, a structure with randomly placed boron and carbon atoms on the anion sites is generated and the atomic positions and lattice vectors are relaxed to equilibrium. These structures are used to approximate the properties of the random alloy. An averaging over disorder is performed by fitting alloy properties to continuous functions of x. Deviations between the properties of the test structures and averaged alloy are observed to be small.

The antifluorite crystal structure that both Be_2B and Be_2C form is cubic. The boron and carbon anions form a close-packed fcc lattice. The beryllium cations form a simple cubic lattice offset by (1/4,1/4,1/4) from the anion lattice that has a lattice constant half that of the anion lattice. The experimental lattice constants[15] of Be_2B and Be_2C are 4.66 and 4.34 Å, which match the DFT lattice constants of 4.57 and 4.33 Å to within 2%. The lattice constant varies linearly with boron concentration upon alloying Be_2B and Be_2C as shown in Fig. 1(a).

The 7% lattice mismatch between Be_2B and Be_2C strains the alloy and leads to a reduction in cohesive energy. The strain energy is calculated by taking the difference in cohesive energies between the $Be_2B_xC_{1-x}$ structures and $xBe_2B+(1-x)Be_2C$ and is plotted in Fig. 1(b). The strain energy of the random alloy can be fit by using the Madelung energy of point ions for the three antifluorite structures,

$$\Delta F_{\text{strain}} = 0.15\frac{x(1-x)}{1+0.055x}\ \text{eV/atom}, \tag{3}$$

with an rms error of 3 meV/atom. There is a small skew to the strain energy not represented by the Madelung model that we correct for by using a least-squares cubic fit,

$$\Delta F_{\text{strain}} = (0.19-0.075x)x(1-x)\ \text{eV/atom}, \tag{4}$$

with a smaller rms error of 1.7 meV/atom. Deviations from the fitting function are caused by the interaction energy between boron and carbon atoms within the test structures. The interaction energy can in principle be fit to a cluster expansion, but these effects are neglected here.

At low temperatures, it is energetically favorable for the $Be_2B_xC_{1-x}$ alloy to reduce lattice strain by phase separating into a boron-rich and carbon-rich alloy. At high temperatures, the uniformly mixed alloy is stabilized by the free-energy contribution from the entropy of mixing of boron and carbon in the anion lattice,

$$\Delta F_{\text{mix}} = \frac{k_BT}{3}[x\ln x+(1-x)\ln(1-x)]\ \text{eV/atom}. \tag{5}$$

Because of the structural similarity of the competing phases, the difference in vibrational free energy is small and can be fit to

$$\Delta F_{\text{vib}} = -x(1-x)\left[0.006+0.5\left(\frac{k_BT}{eV}\right)^2\right]\ \text{eV/atom} \tag{6}$$

with an rms error of 1.6 meV/atom in the range 0–2000 K. The vibrational free-energy contribution favors mixing of the alloy. With the free-energy contributions parametrized as a function of x and T in Eqs. (4)–(6), the mixing-separation phase diagram is calculated in Fig. 1(c). The phase separation region of the phase diagram corresponds to the reaction

$$Be_2B_xC_{1-x} \rightarrow n(T)Be_2B_{x_1(T)}C_{1-x_1(T)} + [1-n(T)]Be_2B_{x_2(T)}C_{1-x_2(T)}, \tag{7}$$

where $x_1(T)$ and $x_2(T)$ are the two points on the phase boundary line at temperature T. The accuracy of the phase diagram is estimated by comparing it to a phase diagram constructed using Eq. (3), which changes phase boundaries by as much as 300 K. According to this approximate phase diagram, the $Be_2B_xC_{1-x}$ alloy can be formed at any boron concentration above 2300 K. This conclusion ignores the competition of other structural phases, which are discussed in Sec. IV.

The phonon band structures for Be_2C and Be_2B and phonon density of states for the $Be_2B_xC_{1-x}$ test structures are plotted in Fig. 2. These band structures show significant differences, mainly resulting from the increased dispersion of the optical modes of Be_2C compared to Be_2B. The densities

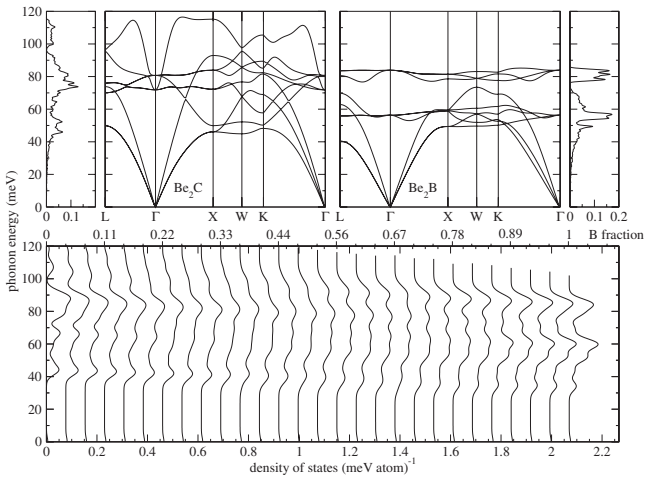

FIG. 2. Calculated phonon properties of antifluorite $Be_2B_xC_{1-x}$. The Be_2B and Be_2C densities of states are plotted with a Gaussian smearing of 0.5 meV. The alloy densities of states are approximated from the Γ point of their supercell and plotted with a Gaussian smearing of 4 meV.

of states of the test structures show a smooth concentration dependence that interpolate between Be_2C and Be_2C without strong disorder-induced variations. The overall trend is toward softer phonons as the boron concentration increases.

The electronic band structures for Be_2C and Be_2B and electronic density of states for the $Be_2B_xC_{1-x}$ test structures are plotted in Fig. 3. The valence bands of Be_2C and Be_2B are very similar, the main difference being their offset from the Fermi level. It is apparent from the alloy densities of states that the $2p$ bands at the Fermi level are uniformly shifted upward as a function of boron concentration. This behavior validates a rigid-band description of boron doping of Be_2C for electronic states at the Fermi level. In contrast, the lowest energy $2s$ band does not appear to hybridize between boron and carbon. The lower carbon $2s$ band disappears with increasing boron concentration as the boron 2s band emerges at a higher energy. The density of states peak

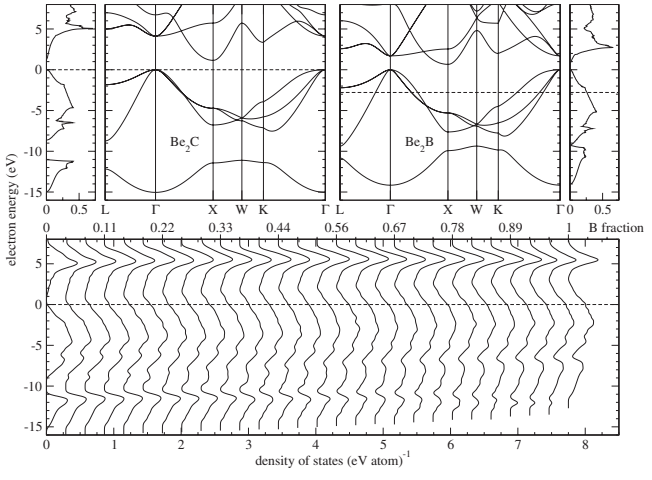

FIG. 3. Calculated electronic properties of antifluorite $Be_2B_xC_{1-x}$. The dashed lines indicate the Fermi energy. The alloy densities of states are plotted with a Gaussian smearing of 0.35 eV.

at 5 eV above the Fermi level remains unchanged with boron concentration and may be a resonance associated with the unfilled $2s$ bands of the beryllium ions.

IV. THERMODYNAMIC STABILITY

If the antifluorite $Be_2B_xC_{1-x}$ alloy is thermodynamically stable within some region of concentration and temperature of the Be-B-C phase diagram, it might allow for a straightforward synthesis of the material. The complete ternary phase diagram of Be-B-C is not at present known,[34] except for the beryllium-poor phases BeB_2C_2 and $BeB_{12}C_2$ and complete Be-B, Be-C, and B-C binary phase diagrams.[15,35] A thermodynamically stable region of antifluorite $Be_2B_xC_{1-x}$ in the phase diagram requires an absence of more stable competing phases. In Sec. III, we have shown that phase separation into boron-rich and carbon-rich alloys already limits the accessible values of x at lower temperatures. Further analysis of the boron-rich antifluorite structure will show that its thermodynamic stability requires the material to be highly defective. This restricts the discussion to the carbon-rich region, within which we estimate the solubility limit of boron.

Within the known Be-B binary phase diagram,[15] Be_2B is thermodynamically stable in the temperature range 1300–1800 K. Be_2B melts above 1800 K, and decomposes according to the reaction

$$Be_2B \rightarrow 0.451Be_4B + 0.197BeB_{2.79}. \quad (8)$$

The structure of Be_4B is a distorted cubic close-packed structure with ordered vacancies[36] and $BeB_{2.79}$ is a boron cage structure encapsulating interstitial beryllium atoms.[37] At zero temperature, our calculations show that this reaction is favorable by 73 meV per atom. At the experimental transition temperature of 1300 K, the reaction is calculated to still be favorable by 64 meV per atom and remains favored up to ~7000 K. A likely reason for this theoretical failure to describe Eq. (8) is that Be_2B forms as a highly defective structure. In this scenario, defects with small or negative formation energies might stabilize the material at a finite temperature with their cohesive energy and configurational entropy contributions to the free energy. For example, the formation energy of a boron vacancy in Be_2B is almost zero and the mixing of boron atoms and vacancies can reduce the free energy by as much as 78 meV per Be_2X unit at 1300 K using Eq. (5). This single defect type is not enough to stabilize the Be_2B phase but it demonstrates the plausibility of the defect scenario. Possible experimental evidence for this scenario is the measurement[16] of a beryllium to boron ratio of 2.8 to 1 in a sample of the Be_2B phase. The experimental deviation from ideal stoichiometry indicates the presence of boron vacancies or more complicated defect structures. Since the exact nature of defects in thermodynamically synthesized Be_2B is unclear, we cannot study the superconducting properties of the defective phase.

The presence of carbon may help to reduce defects in Be_2B because of the increased stability of Be_2C. For the simple case of an isolated boron vacancy, we consider the energy gained from filling the vacancy with a carbon atom. Using the same supercell as in the alloy calculations, we

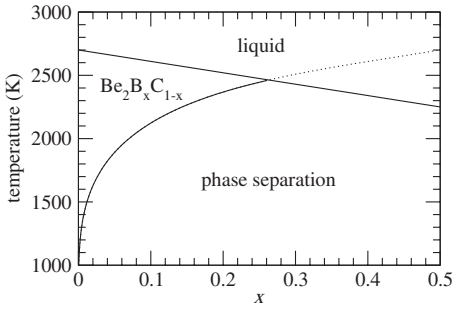

FIG. 4. Estimated phase diagram of $Be_2B_xC_{1-x}$. Phase separation boundary is calculated considering Be_4B, $BeB_{2.79}$, and antifluorite $Be_2B_xC_{1-x}$. Solid-liquid phase boundary is linearly interpolated from the melting points of Be_2B and Be_2C.

calculate that a carbon atom reduces its energy by 1.1 eV in going from graphite to filling a vacancy in $Be_{54}B_{26}$ to form $Be_{54}B_{26}C$. The configurational entropy is left unchanged, replacing boron-vacancy mixing with boron-carbon mixing within the anion lattice. Any remaining vacancies may further increase the configurational entropy by mixing three components, boron-carbon-vacancy.

The Be_2C phase has been studied more than the Be_2B phase and there are experimental reports of thermodynamic synthesis of single crystals with no observed defects.[17] The Be-C phase diagram is much simpler than Be-B, with no competing solid phases. Above 2500 K, Be_2C begins to decompose into graphite and gaseous beryllium, and above 2700 K, Be_2C melts.[15] We assume that defects are not important in the carbon-rich limit of the antifluorite $Be_2B_xC_{1-x}$ alloy. To estimate the solubility of boron within Be_2C, we consider the reaction

$$Be_2B_xC_{1-x} \rightarrow (1-x)Be_2C + x(0.451Be_4B + 0.197BeB_{2.79}). \tag{9}$$

The free-energy model of $Be_2B_xC_{1-x}$ from Sec. III is used for the calculation. Since this decomposition is more energetically favorable than isostructural phase separation within the antifluorite structure, the solubility of boron is reduced from Fig. 1(c). Considering the competition of the three solid phases and the liquid phase, an approximate phase diagram is plotted in Fig. 4. The decomposition to graphite and beryllium gas is omitted as it may be forced to higher temperatures at elevated pressures. This phase diagram is a crude estimate that does not properly account for the liquid phase or other solid phases. The melting temperature of $Be_2B_xC_{1-x}$ as a function of x is not known, but Be_2B and Be_2C melt at 1800 and 2700 K.[15] It is known empirically[38] that melting points of alloys can be linearly interpolated from the melting points of their constituents. For example, the melting points of elemental Be, B, and C are 1600, 2400, and 3900 K, and interpolation gives reasonable melting temperatures of 1900 and 2400 K for Be_2B and Be_2C. This motivates the linear interpolation of the melting points of Be_2B and Be_2C to estimate the melting temperature of $Be_2B_xC_{1-x}$.

From the phase diagram in Fig. 4, we estimate that antifluorite $Be_2B_xC_{1-x}$ is thermodynamically accessible in the range $0 \leq x \leq 0.25$ through high-temperature synthesis. At ambient temperatures, $Be_2B_xC_{1-x}$ is thermodynamically unstable, but it is structurally stable as shown in Sec. III. The alloy should persist as a metastable phase until phase separation occurs. The rate of phase separation is determined by the diffusion of boron and carbon atoms within the antifluorite structure and is beyond the scope of this paper.

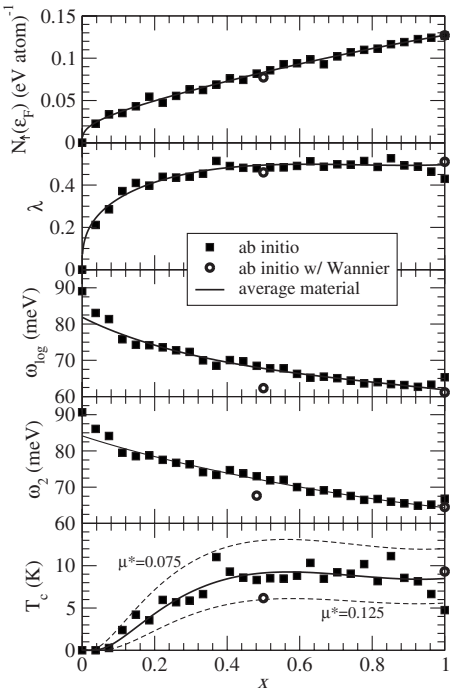

FIG. 5. Calculated values of $N_\uparrow(\epsilon_F)$, λ, $\omega_{\log}$, ω_2, and T_c for antifluorite $Be_2B_xC_{1-x}$.

V. SUPERCONDUCTING PROPERTIES

We study the superconducting properties of antifluorite $Be_2B_xC_{1-x}$ using the same 28 supercell structures as in Sec. III. The values of λ, $\omega_{\log}$, ω_2, and T_c calculated using the approximate Eliashberg spectral function $\alpha^2F_\Gamma(\omega)$ of Eq. (1) are plotted in Fig. 5. As in the boron-doped diamond case,[6] it is assumed that $\alpha^2F_\Gamma(\omega)$ of the random alloy is a smooth function of boron concentration that is approximated by $\alpha^2F_\Gamma(\omega)$ of the calculated structures. The value of $\alpha^2F_\Gamma(\omega)$ is linearly proportional to the electronic density of states per spin at the Fermi level, $N_\uparrow(\epsilon_F)$, which goes as the cubic root of boron concentration near the band edge for parabolic bands in three dimensions. To account for this concentration dependence and average over disorder, $N_\uparrow(\epsilon_F)$ is least-squares fit to the functional form

$$f(x) = x^{1/3}(f_0 + f_1x + f_2x^2 + f_3x^3). \tag{10}$$

The quantities λ, $\lambda \log(\omega_{\log})$, and $\lambda\omega_2^2$ are all linear in $\alpha^2F_\Gamma(\omega)$ and are also least-squares fit to this functional form.

The average T_c values in Fig. 5 are calculated based on the averaged values of λ and $\omega_{\log}$ and a μ^* of 0.1. There is a broad plateau of T_c near 9 K for boron concentrations greater than 40%, with a slight dip at higher boron concentrations due to a gradual reduction in $\omega_{\log}$. Because this material is in

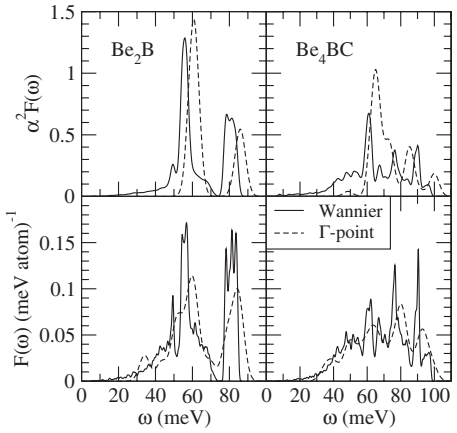

FIG. 6. Comparison of $\alpha^2F(\omega)$ and $F(\omega)$ for Be_2B and Be_4BC between the Γ-point approximation (4 meV Gaussian smearing) and the Wannier-based calculation (0.5 meV Gaussian smearing).

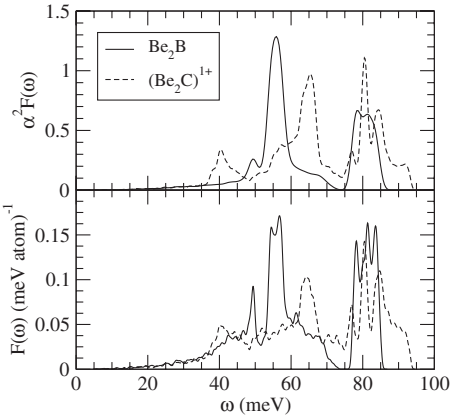

FIG. 7. Comparison of $\alpha^2F(\omega)$ and $F(\omega)$ for Be_2B and rigid-band hole-doped Be_2C each with seven valence electrons per formula unit. This data is plotted with a 0.5 meV Gaussian smearing.

the weak-coupling regime, the T_c values are very sensitive to errors in λ and μ^*, changing by ~ 1 K per 0.01 deviation in either quantity within this parameter range. This sensitivity is illustrated in Fig. 5 by calculating T_c for slightly smaller and larger values of μ^*. With the fluctuations observed in the calculations and uncertainty in μ^*, a safe window of prediction for the maximum value of T_c is 5–13 K. The value of μ^* is not expected to have a strong dependence on boron concentration and with a smooth x dependence of λ and $\omega_{\log}$, the random alloy should retain this plateau feature in T_c versus x despite the uncertainty in the value of the T_c plateau.

To clarify the accuracy of our superconductivity calculations based on $\alpha^2F_\Gamma(\omega)$, we compare them with precise Wannier-based calculations of $\alpha^2F(\omega)$ for two small representative systems. These systems are Be_2B and Be_4BC constructed as a $2\times1\times1$ supercell of the primitive antifluorite unit cell with one boron and one carbon anion. The calculation of $\alpha^2F_\Gamma(\omega)$ for Be_4BC is performed using a $2\times3\times3$ supercell of the original supercell. A comparison of the spectral functions and phonon densities of states $F(\omega)$ is plotted in Fig. 6 and the Wannier results are included in Fig. 5. For both systems, there is a small contribution from the acoustic part of the spectrum below 50 meV that is absent from the Γ-point approximation. The overall trend is that while $F(\omega)$ for the Γ-point approximation is reasonably accurate, there is a visible shift in $\alpha^2F_\Gamma(\omega)$ to higher phonon frequencies compared to $\alpha^2F(\omega)$. This shift leads to an overestimate of $\omega_{\log}$, from 61 to 65 meV for Be_2B and from 62 to 71 meV for Be_4BC, and an underestimate of λ, from 0.51 to 0.43 for Be_2B and from 0.46 to 0.44 for Be_4BC. The result is an underestimation of T_c values, from 9.3 to 4.7 K for Be_2B and 6.1 to 5.7 K for Be_4BC. The integrated quantity $\sqrt{\lambda\langle\omega^2\rangle}$ is independent of details of the phonon spectrum[10] and represents the total coupling of electrons at the Fermi surface to atomic perturbations. There is no observed systematic error in $\sqrt{\lambda\langle\omega^2\rangle}$ between $\alpha^2F(\omega)$ and $\alpha^2F_\Gamma(\omega)$, calculated to be 46 and 44 meV for Be_2B and 46 and 48 meV for Be_4BC. We conclude that $\alpha^2F_\Gamma(\omega)$ is a good estimate of total electron-phonon coupling strength for $Be_2B_xC_{1-x}$, but shifts in coupling to higher phonon frequencies lead to a systematic underestimate of λ and overestimate of $\omega_{\log}$. This may lead to a systematic underestimation of our predicted T_c values from the Γ-point approximation $Be_2B_xC_{1-x}$ calculations.

It is often assumed that there is a proportionality between $N_\uparrow(\epsilon_F)$ and λ, which leads to a common decomposition $\lambda = N_\uparrow(\epsilon_F)V_{ep}$ and a design principle of raising T_c by increasing $N_\uparrow(\epsilon_F)$. From Fig. 5 it is clear that such a principle cannot be employed for $Be_2B_xC_{1-x}$, as λ saturates near 0.5 while $N_\uparrow(\epsilon_F)$ grows linearly with boron concentration. A more detailed decomposition[27] of λ is

$$\lambda = \sum_i \frac{N_\uparrow(\epsilon_F)\langle I_i^2\rangle}{M_i\omega_2^2}, \tag{11}$$

where the sum is over atomic species, M_i are the nuclear masses, $\langle I_i^2\rangle$ are the electron-phonon matrix elements averaged over the Fermi surface, and ω_2 is an average phonon frequency that is plotted for the test structures and random alloy in Fig. 5. Considering the doping dependence of $N_\uparrow(\epsilon_F)$ and ω_2, the overall electron-phonon coupling strength $\Sigma_i\langle I_i^2\rangle/M_i$ decreases by $\sim 80\%$ in going from Be_2C to Be_2B. The matrix elements in $\langle I_i^2\rangle$ contain pairs of electronic states on the Fermi surface and a screened dipole potential induced by atomic perturbations of atoms of species i. Doping must significantly alter the screened potential, the electronic states, or both.

The chemical effects of doping can be distinguished by comparing the properties of Be_2B with hole-doped Be_2C, both containing seven valence electrons per formula unit. Be_2C is doped by shifting the Fermi level and compensating the positive charge of the unit cell with a uniform negative charge background. Using the Wannier function approach, $\alpha^2F(\omega)$ and the phonon density of states $F(\omega)$ are calculated for these two systems and plotted in Fig. 7. There is a clear trend of phonon softening in both Be_2B and hole-doped Be_2C compared to the undoped insulating Be_2C in Fig. 2. For both Be_2B and hole-doped Be_2C there is a correspondence of features in $\alpha^2F(\omega)$ and $F(\omega)$. Comparing Be_2B to

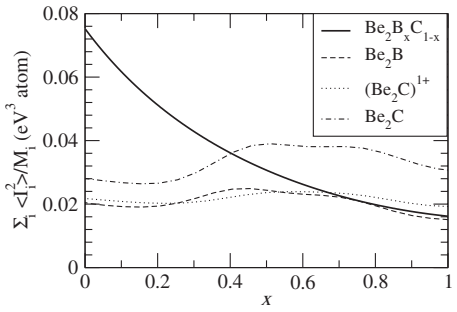

FIG. 8. Comparison of $\Sigma_i\langle I_i^2\rangle/M_i$ for Be_2B, hole-doped Be_2C, undoped Be_2C, and the $Be_2B_xC_{1-x}$ alloy. For $Be_2B_xC_{1-x}$, the x axis corresponds to boron concentration. For the remaining materials, the x axis corresponds to electron-phonon properties calculated using Eq. (1) for varying energy surfaces $\epsilon(x)$. These surfaces are chosen such that the total number of valence electrons per Be_2X integrated up to $\epsilon(x)$ is $8-x$.

hole-doped Be_2C, Be_2B has high-frequency optical modes of narrower bandwidth and shifts in its mid-frequency peak from ~65 to ~55 meV. To understand the effect of these differences on superconducting properties, we make comparisons of relevant integrated quantities. Be_2B is calculated to have $\lambda=0.51$, $\omega_2=65$ meV, and $N_\uparrow(\epsilon_F)=0.13$ states/(eV atom). Hole-doped Be_2C is calculated to have $\lambda=0.61$, $\omega_2=69$ meV, and $N_\uparrow(\epsilon_F)=0.16$ states/(eV atom). If λ is decomposed as in Eq. (11), then the average electron-phonon matrix element $\Sigma_i\langle I_i^2\rangle/M_i$ is reduced by ~10% in going from hole-doped Be_2C to Be_2B. The chemical differences between boron and carbon account for only a small part of the reduction in electron-phonon coupling with boron doping.

Another possible difference in $\langle I_i^2\rangle$ between Be_2C and Be_2B is the additional metallic screening of the dipole potential due to a large $N_\uparrow(\epsilon_F)$ in Be_2B. To avoid chemical differences, we study this possibility by comparing the $\alpha^2F_\Gamma(\omega)$ of hole-doped Be_2C to insulating Be_2C with Eq. (1) evaluated for an energy surface ϵ instead of ϵ_F. This ϵ is chosen such that the electron density of states per Be_2X integrated up to ϵ is 7, the same number of valence electrons as in the hole-doped material. The difference in $\langle I_i^2\rangle$ between these test systems should be contained mainly within their screened potentials, since the electronic states considered should be similar. If screening caused by electrons at the Fermi surface is a large effect, then the electron-phonon matrix elements in Eq. (1) should be very different for these two calculations since insulating Be_2C has no Fermi surface and thus no metallic screening. These two systems also have small differences in their self-consistent potentials, which lead to small changes in the band structure and electronic states. The result of the calculation is that $\lambda=0.48$, $\omega_2=79$ meV, and $N_\uparrow(\epsilon_F)=0.16$ states/(eV atom) with metallic screening and $\lambda=0.47$, $\omega_2=96$ meV, and $N_\uparrow(\epsilon_F)=0.14$ states/(eV atom) without metallic screening. Metallic screening leads to a ~40% reduction in $\Sigma_i\langle I_i^2\rangle/M_i$ compared to the system with similar electronic states but no metallic screening. This has a larger effect than the chemical difference between boron and carbon.

The final contributions to $\langle I_i^2\rangle$ to consider are the electronic states used in the matrix elements. To separate this effect from variations in the screened potential, we vary the energy surface on which Eq. (1) is evaluated for a given material. In Fig. 8, the value of $\Sigma_i\langle I_i^2\rangle/M_i$ is evaluated for varying energy surfaces of Be_2B, Be_2C, and hole-doped Be_2C. The variations in $\Sigma_i\langle I_i^2\rangle/M_i$ within this energy range are on the order of 20%, but there is no definite trend with doping. In contrast, there is a steady decline of $\Sigma_i\langle I_i^2\rangle/M_i$ in $Be_2B_xC_{1-x}$ as a function of x. We conclude that the electronic states on these energy surfaces do not approximate the states on the Fermi surfaces of $Be_2B_xC_{1-x}$. This deviation may be the result of localization caused by varying on-site potentials between boron and carbon in $Be_2B_xC_{1-x}$. Such localization has been theoretically shown to increase electron-phonon coupling.[39] In this class of materials, the net effect of this coupling enhancement is to expedite the onset of superconductivity as a function of boron concentration, without changing the maximum attainable T_c.

VI. CONCLUSIONS

Our calculations suggest that $Be_2B_xC_{1-x}$ in the antifluorite structure is thermodynamically stable at high temperatures in the range $0\leq x\leq 0.25$. This alloy is predicted to be a superconductor when boron is introduced. For the most boron-rich phase that is likely to be accessed by high-temperature synthesis, $x=0.25$, the transition temperature is predicted to be in the range 3–8 K. At higher boron concentrations, $x\geq 0.4$, T_c is predicted to plateau somewhere in the range 5–13 K. As is the case in boron-doped diamond,[5] achieving these higher T_c values may be possible through nonequilibrium synthesis techniques such as chemical-vapor deposition. The predicted transition temperature is small compared to the 40 K observed in MgB_2 (Ref. 1) and the 80 K predicted to be the limit in boron-doped diamond.[6] The reduced T_c compared to other boron-containing structures is because $Be_2B_xC_{1-x}$ remains in the weak-coupling regime of superconductivity. Even with boron-carbon substitution acting as a flexible tuning parameter of electronic properties in $Be_2B_xC_{1-x}$ and the large value of $N_\uparrow(\epsilon_F)$ attainable, the value of λ saturate near 0.5.

The overall reduced magnitude of electron-phonon coupling in $Be_2B_xC_{1-x}$ may be attributed to the ionic antifluorite structure lacking in the strong covalent bonding of the sp^2 graphitic plane of MgB_2 or sp^3 framework of diamond. One advantage of $Be_2B_xC_{1-x}$ over boron-doped diamond is that all substituted boron uniformly contributes free carriers and increases $N_\uparrow(\epsilon_F)$. In diamond, neighboring substituted boron atoms can lead to deep acceptor states[40] that cause large variations in $N_\uparrow(\epsilon_F)$ between simulated microscopic configurations.[6] This study cannot rule out the possibility of competing phases that may thermodynamically destabilize antifluorite $Be_2B_xC_{1-x}$ or defects that might compensate free carriers and destroy superconductivity. These problems become more relevant with increasing boron concentration, originating from the many stable Be-B solid phases[15] and experimental uncertainties of the Be_2B phase.[16] Experimental verification remains as the test of the predictions made in this paper.

ACKNOWLEDGMENTS

This work was supported by National Science Foundation Grant No. DMR07-05941 and by the Director, Office of Science, Office of Basic Energy Sciences, Division of Materials Sciences and Engineering Division, U.S. Department of Energy under Contract No. DE-AC02-05CH11231. Calculations in this work were done using the QUANTUM-ESPRESSO package.[31]

*jmoussa@civet.berkeley.edu

[1] J. Nagamatsu, N. Nakagawa, T. Muranaka, Y. Zenitani, and J. Akimitsu, Nature (London) **410**, 63 (2001).
[2] E. A. Ekimov, V. A. Sidorov, E. D. Bauer, N. N. Mel'nik, N. J. Curro, J. D. Thompson, and S. M. Stishov, Nature (London) **428**, 542 (2004).
[3] E. Bustarret, E. C. Marcenat, P. Achatz, P. J. Kacmarcik, J. F. Levy, A. Huxley, L. Ortega, E. Bourgeois, X. Blase, X. D. Debarre, and J. Boulmer, Nature (London) **444**, 465 (2006).
[4] Z.-A. Ren, J. Kato, T. Muranaka, J. Akimitsu, M. Kriener, and Y. Maeno, J. Phys. Soc. Jpn. **76**, 103710 (2007).
[5] Y. Takano, T. Takenouchi, S. Ishii, S. Ueda, T. Okutsu, I. Sakaguchi, H. Umezawa, H. Kawarada, and M. Tachiki, Diamond Relat. Mater. **16**, 911 (2007).
[6] J. E. Moussa and M. L. Cohen, Phys. Rev. B **77**, 064518 (2008).
[7] M. Calandra, N. Vast, and F. Mauri, Phys. Rev. B **69**, 224505 (2004).
[8] M. Calandra, A. N. Kolmogorov, and S. Curtarolo, Phys. Rev. B **75**, 144506 (2007).
[9] H. Rosner, A. Kitaigorodsky, and W. E. Pickett, Phys. Rev. Lett. **88**, 127001 (2002).
[10] W. L. McMillan, Phys. Rev. **167**, 331 (1968).
[11] J. P. Goss and P. R. Briddon, Phys. Rev. B **73**, 085204 (2006).
[12] H. Mukuda, T. Tsuchida, A. Harada, Y. Kitaoka, T. Takenouchi, Y. Takano, M. Nagao, I. Sakaguchi, T. Oguchi, and H. Kawarada, Phys. Rev. B **75**, 033301 (2007).
[13] M. M. Balakrishnarajan, P. D. Pancharatna, and R. Hoffmann, New J. Chem. **31**, 473 (2007).
[14] A. M. Fogg, J. Meldrum, G. R. Darling, J. B. Claridge, and M. J. Rosseinsky, J. Am. Chem. Soc. **128**, 10043 (2006).
[15] H. Okamoto and L. E. Tanner, in *Phase Diagram of Binary Beryllium Alloys*, edited by H. Okamoto and L. E. Tanner (ASM, Metals Park, OH, 1987), pp. 21 and 31.
[16] L. A. J. Garvie, P. R. Buseck, and P. Rez, J. Solid State Chem. **133**, 347 (1997).
[17] C.-T. Tzeng, K.-D. Tsuei, and W.-S. Lo, Phys. Rev. B **58**, 6837 (1998).
[18] I. R. Shein and A. L. Ivanovskii, Phys. Status Solidi B **227**, R1 (2001).
[19] I. R. Shein and A. L. Ivanovskii, J. Struct. Chem. **46**, 535 (2005).
[20] J. L. Corkill and M. L. Cohen, Phys. Rev. B **48**, 17138 (1993).
[21] P. B. Allen and B. Mitrović, Solid State Phys. **37**, 2 (1982).
[22] G. Kresse and J. Furthmüller, Phys. Rev. B **54**, 11169 (1996).
[23] P. E. Blöchl, Phys. Rev. B **50**, 17953 (1994).
[24] J. P. Perdew, K. Burke, and M. Ernzerhof, Phys. Rev. Lett. **77**, 3865 (1996).
[25] D. M. Wood and A. Zunger, Phys. Rev. B **34**, 4105 (1986).
[26] S. Lupi, L. Baldassarre, M. Ortolani, P. Calvani, U. Schade, and Y. Takano, Phys. Status Solidi A **204**, 2945 (2007).
[27] P. B. Allen and R. C. Dynes, Phys. Rev. B **12**, 905 (1975).
[28] P. Morel and P. W. Anderson, Phys. Rev. **125**, 1263 (1962).
[29] J. E. Moussa and M. L. Cohen, Phys. Rev. B **74**, 094520 (2006).
[30] F. Giustino, M. L. Cohen, and S. G. Louie, Phys. Rev. B **76**, 165108 (2007).
[31] S. Baroni, A. Dal Corso, S. de Gironcoli, P. Giannozzi, C. Cavazzoni, G. Ballabio, S. Scandolo, G. Chiarotti, P. Focher, A. Pasquarello, K. Laasonen, A. Trave, R. Car, N. Marzari, and A. Kokalj, http://www.pwscf.org/.
[32] P. Souvatzis, O. Eriksson, M. I. Katsnelson, and S. P. Rudin, Phys. Rev. Lett. **100**, 095901 (2008).
[33] G. D. Garbulsky and G. Ceder, Phys. Rev. B **53**, 8993 (1996).
[34] P. Rogl, in *Phase Diagrams of Ternary Metal-Boron-Carbon Systems*, edited by G. Effenberg (ASM, Metals Park, OH, 1998), p. 18.
[35] H. Okamoto, in *Binary Alloy Phase Diagrams*, 2nd ed., edited by T. B. Massalski (ASM, Metals Park, OH, 1990), p. 464.
[36] H. J. Becher and A. Schafer, Z. Anorg. Allg. Chem. **318**, 304 (1962).
[37] J. Y. Chan, F. R. Fronczek, D. P. Young, J. F. DiTusa, and P. W. Adams, J. Solid State Chem. **163**, 385 (2002). There remains some uncertainty in the crystal structure due to fractional occupancy of some lattice sites. We choose B7 and B8/Be8 occupancies to match the ordering proposed in the text. The half-filled Be12 sites locally form the vertices of a hexagon and are filled to maximize the Be-Be distance, forming the vertices of an equilateral triangle. We consider only a single unit cell of the crystal within which the fractional occupancy of the Be13 site cannot be modeled. With respect to phase separation toward Be_4B, it is energetically favorable to have the Be13 sites empty at zero temperature, considering only integer occupations. This leaves us with a unit cell containing 29 Be atoms and 81 B atoms. Configurational entropy is likely to stabilize a partial occupation of the Be13 sites at elevated temperatures. At the experimental occupation of 0.125 on the Be13 sites, the configurational free-energy contribution is less than 2 meV per atom in the temperature range of interest and is ignored.
[38] J. R. Chelikowsky and K. E. Anderson, J. Phys. Chem. Solids **48**, 197 (1987).
[39] R. Atta-Fynn, P. Biswas, and D. A. Drabold, Phys. Rev. B **69**, 245204 (2004).
[40] E. Bourgeois, E. Bustarret, P. Achatz, F. Omnès, and X. Blase, Phys. Rev. B **74**, 094509 (2006).